A multi-phase cohesive segments method for the simulation of self-healing materials

A MULTI-PHASE COHESIVE SEGMENTS METHOD FOR THE SIMULATION OF SELF-HEALING MATERIALS

Delft University of Technology, Faculty of Aerospace Engineering

PO Box 5058, Delft, The Netherlands

J.J.C.Remmers@TUDelft.nl , R.deBorst@TUDelft.nl

The backbone of a numerical technique for the simulation of self-healing mechanisms is the cohesive segments method. This method, which is based on the partition of unity method, allows for the simulation of multiple interacting cracks in a heterogeneous medium, irrespective of the structure of the finite element mesh. In this paper, a concise overview of the cohesive segments method is given. The performance of the method is illustrated with an example.

Keywords: Numerical analysis, fracture mechanics, cohesive segments method, partition of unity method

1 Introduction

One of the most promising techniques to accomplish self-healing in polymer composites is the micro-encapsulation of a healing agent in combination with a chemical catalyst within the epoxy matrix [1]. When a crack in the epoxy material ruptures the micro-capsule, the healing agent will be released into the crack due to capillary action. The catalysts trigger polymerisation of the healing agent, which will bond the crack surfaces in order to restore the load carrying capability of the material.

Clearly, the efficiency of the method relies on the speed of the chemical reaction, the cohesive strength of the polymerised material and the adhesive strength of the polymer-epoxy interface. Other factors that play an important role are the distribution of the healing agent into the crack and the probability that the agent reacts with a catalyst. Due to the complexity of the problem and the large number of variables, it is essential to develop a simulation tool to obtain a detailed understanding of the role played by each component of the system as well as the interaction between physical processes. This knowledge can be achieved through numerical simulations that explicitly model the distribution of catalysts and micro-capsules and the flow of the healing agent through a crack on a microscopic level of observation.

The simulation tool that is proposed here, is composed of state of the art numerical techniques. First, the evolution of micro-cracks can be simulated by the cohesive segments method [2] which is an extension of the partition of unity approach to cohesive fracture [3,4]. The cohesive segments method is able to simulate the nucleation, growth and coalescence of multiple interacting cracks, irrespective of the structure of the underlying finite element mesh. The subsequent flow of fluids through the deformable, porous media is governed by a classical two-phase theory [5]. A partition of unity extension of this model accounts for the flow of fluids through the cracks by capillary action [6].

The final stage of the healing process, the rebonding of the crack surfaces, is simulated by a reversed cohesive constitutive model [7], in which the strength of the cohesive zone is restored as function of time.

In this paper, the attention is restricted to the first part of the numerical tool, the cohesive segments method. After a short introduction, the basic kinematic relations are presented, followed by the derivation of the momentum balance equations. Some important aspects regarding the implementation of the method in a finite element code are discussed as well. The paper is concluded with a small example to demonstrate the performance of the method.

2 The simulation of fracture

In the cohesive zone approach to fracture, the process zone is lumped in a single plane or line ahead of the existing crack, [8,9]. The relation between the work expended in this cohesive zone and that in the crack tip field is typically such that the stress singularity is cancelled and the near tip stresses in the process zone are finite. Needleman [10] extended the approach by inserting cohesive constitutive relations at specified planes in the materials, whether or not there is a crack. Apart from the fact that this approach can capture crack nucleation, there is an additional technical advantage. By specifying the cohesive relation along a surface, there is no need to determine the length of the cohesive zone.

An independent constitutive relation that describes the separation of the cohesive surface governs the failure characteristics of the material. This cohesive constitutive relation, together with the constitutive relation for the bulk material and the appropriate balance laws and boundary and initial conditions, completely specify the problem. Fracture, if it takes place, emerges as a natural outcome of the deformation process without introducing any additional failure criterion.

Conventionally, the cohesive surfaces have been incorporated in the finite element mesh beforehand by means of interface elements that are placed between the standard continuum elements. These elements consist of two surfaces that are connected to the adjacent continuum elements. A perfect bond prior to cracking is simulated by applying a high dummy stiffness to the interface elements. In cases when fracture takes place along well-defined interfaces as, for example in a lamellar solid, the placement of interface elements in the finite element mesh is clear. However, for a solid that is homogeneous on the scale modelled, the crack path is often not known and the placement of cohesive surfaces can be problematic. To allow for crack growth in arbitrary directions, interface elements are placed between all continuum elements in the mesh [11]. This approach enables the simulation of complex fracture phenomena such as crack initiation away from the crack tip and crack branching [12], see Figure1. Alternatively, Tijssens et al. [13] have been using the method to simulate nucleation and coalescence of micro-cracks in the micro-structure of heterogeneous materials.

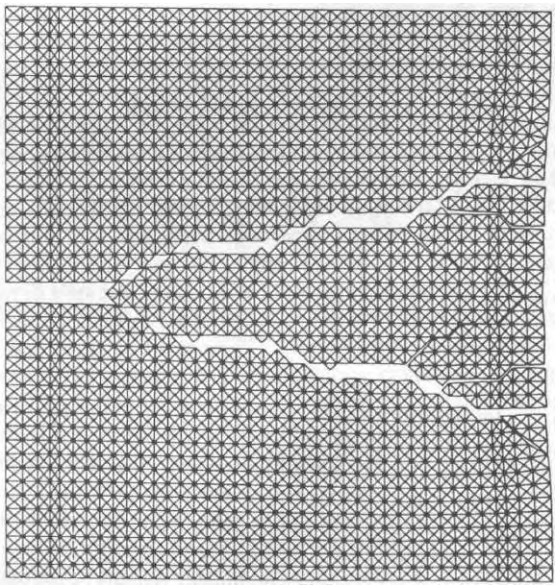

Figure 1: Simulation of crack branching in Polymethyl Methacrylate (PMMA) using inter-element cohesive surface models [12]. Note that although the crack can only propagate in the 0°, $\pm 45^\circ$ and 90° directions, the propagation in other directions is captured relatively well.

Unfortunately, the approach of placing interfaces between all continuum elements is not completely mesh independent. In fact, since the interface elements are aligned with element boundaries, the orientation of cracks is restricted to a limited number of angles. In addition, if the initial compliance is taken to be non-zero, the presence of the interfaces contributes to the overall compliance of the body which has an ill-posed problem as a result. Increasing the dummy stiffness, which describes the elastic behaviour of the cohesive zone prior to fracture, can reduce the magnitude of this error. Unfortunately, in most cases, high dummy stiffnesses can give rise to numerical problems [14].

In order to avoid these finite element mesh related problems, the cohesive surface is incorporated in the continuum elements by using the partition-of-unity property of finite element shape functions [15] in conjunction with a discontinuous mode incorporated at the element level [3]. In this approach, the cohesive zone is represented by a jump in the displacement field of the continuum elements [4]. The magnitude of the displacement field is determined by an additional set degrees of freedom, which is added to the existing nodes of the finite element mesh. A crack (or cohesive surface) can be extended during the simulation at any time and in any direction, irrespective of the structure of the underlying finite element mesh. In addition, most numerical problems that are related to the initial dummy stiffness are avoided since the cohesive zone is only inserted upon crack propagation. Finally, an important advantage over traditional remeshing techniques is that the topology of the finite element mesh is not modified: the number of nodes and elements remains the same, as well as their mutual connectivity.

In order to accommodate the simulation of multiple interaction crack patterns, the aforementioned partition of unity approach to cohesive fracture has been extended to the cohesive segments method in which multiple discontinuities are defined [2]. Since each part is supported by a unique additional set of degrees of freedom, the interaction between different cracks can be modelled as well.

The cohesive segments method can be used to simulate both the interfaces between the different constituents in the material, as well as the cohesive fracture in the bulk material.

3 Kinematic relations

The key feature of the partition of unity based approaches to cohesive fracture is that the discontinuity that represent the cohesive zone is incorporated in the kinematic relation that forms the basis of the element formulation. Consider the body Ω in Figure 2 that is crossed by m discontinuities $\Gamma_{\mathrm{d},j}$ that do not intersect.

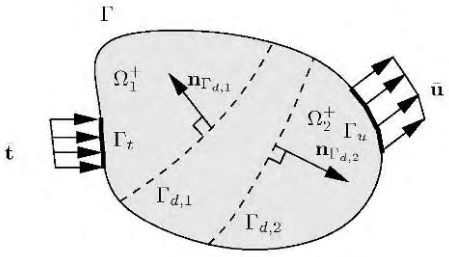

Figure 2: Domain Ω with two discontinuities, $\Gamma_{\mathrm{d},1}$ and $\Gamma_{\mathrm{d},2}$ (dashed lines). It is assumed that the discontinuities do not cross.

Each discontinuity splits the body in two parts, denoted by Ω_j^+ and Ω_j^-. The total displacement of a material point $\mathbf{x}$ in the body consists of a regular part $\hat{\mathbf{u}}$ plus m additional parts $\tilde{\mathbf{u}}_j$ that are added on the side of the corresponding discontinuity $\Gamma_{\mathrm{d},j}$ only:

$$\mathbf{u}(\mathbf{x},t) = \hat{\mathbf{u}}(x,t) + \sum_{j=1}^{m} \mathcal{H}_{\Gamma_{\mathrm{d},j}}(\mathbf{x})\tilde{\mathbf{u}}_j(\mathbf{x},t), \qquad (1)$$

where $\mathcal{H}_{\Gamma_{\mathrm{d},j}}(\mathbf{x})$ is the Heaviside jump function associated with discontinuity j, which is equal to one when x resides in the Ω_j^+ part of the domain and equal to zero when this point is in the Ω_j^-. Assuming a small strain formulation, the strain field can be obtained by differentiating equation (1) with respect to the position $\mathbf{x}$:

$$\boldsymbol{\varepsilon}(\mathbf{x},t) = \nabla^s\hat{\mathbf{u}}(\mathbf{x},t) + \sum_{j=1}^{m} \mathcal{H}_{\Gamma_{\mathrm{d},j}}(\mathbf{x})\nabla^s\tilde{\mathbf{u}}_j(\mathbf{x},t) \qquad \mathbf{x} \notin \Gamma_{\mathrm{d},j}, \qquad (2)$$

where a superscript s denotes the symmetric part of a differential operator. Note that at the discontinuities $\Gamma_{\mathrm{d},j}$, the strains are not defined. There, the magnitude of the displacement jump

$$\mathbf{v}_j(\mathbf{x},t) = \tilde{\mathbf{u}}_j(\mathbf{x},t), \qquad (3)$$

is the relevant kinematic quantity.

4 Momentum balance

The discontinuous displacement and strain fields can be used as an input for the quasi-static equilibrium equations without body forces:

$$\nabla \cdot \boldsymbol{\sigma} = \mathbf{0} \qquad x \in \Omega, \qquad (4)$$

where $\boldsymbol{\sigma}$ is the Cauchy stress in the bulk material.

$$\mathbf{n}_t \cdot \boldsymbol{\sigma} = \bar{\mathbf{t}} \qquad \mathbf{x} \in \Gamma_t, \qquad (5)$$

$$\mathbf{u} = \bar{\mathbf{u}} \qquad \mathbf{x} \in \Gamma_u, \qquad (6)$$

$$\mathbf{n}_{\mathrm{d},j} \cdot \boldsymbol{\sigma} = \mathbf{t}_j \qquad \mathbf{x} \in \Gamma_{\mathrm{d},j}, \qquad (7)$$

where $\bar{\mathbf{t}}$ are the prescribed tractions on Γ_t with outward normal vector $\mathbf{n}_t$, $\bar{\mathbf{u}}$ are the prescribed displacements on Γ_u and $\mathbf{t}_j$ are the tractions at discontinuity $\Gamma_{\mathrm{d},j}$, which can be regarded as an internal boundary. The normal $\mathbf{n}_{d,j}$ at discontinuity $\Gamma_{\mathrm{d},j}$ points into Ω_j^+.

The weak form of the equilibrium equation can be obtained by multiplying equation (4) by an admissible displacement field $\delta\mathbf{u}$. By taking the space of the admissible variations to be the same as the actual displacement field, equation (1), the variations of the displacements can be decomposed as:

$$\delta\mathbf{u} = \delta\hat{\mathbf{u}} + \sum_{j=1}^{m} \mathcal{H}_{\Gamma_{\mathrm{d},j}} \delta\tilde{\mathbf{u}}_j. \qquad (8)$$

Applying Gauss' theorem, using the symmetry of the Cauchy stress tensor and using the boundary conditions at the external boundary Γ_t and at the discontinuity planes $\Gamma_{\mathrm{d},j}$ gives the following equilibrium equations in weak form:

$$\int_\Omega \nabla^s \delta\hat{\mathbf{u}} : \boldsymbol{\sigma} \mathrm{d}\Omega + \sum_{j=1}^{m} \int_\Omega \mathcal{H}_{\Gamma_{\mathrm{d},j}} \nabla^s \delta\tilde{\mathbf{u}}_j : \boldsymbol{\sigma} \mathrm{d}\Omega + \sum_{j=1}^{m} \int_{\Gamma_{\mathrm{d},j}} \delta\tilde{\mathbf{u}}_j \cdot \mathbf{t}_j \mathrm{d}\Gamma =$$
$$\int_{\Gamma_t} \delta\hat{\mathbf{u}} \cdot \bar{\mathbf{t}} \mathrm{d}\Gamma + \sum_{j=1}^{m} \int_{\Gamma_t} \mathcal{H}_{\Gamma_{\mathrm{d},j}} \delta\tilde{\mathbf{u}}_j \cdot \bar{\mathbf{t}} \mathrm{d}\Gamma. \qquad (9)$$

Note that the weak form of equilibrium equation can be split in $j+1$ individual equations by taking one term of the admissible displacement field (either $\delta\hat{\mathbf{u}}$ or $\delta\tilde{\mathbf{u}}_j$) at a time while setting the remaining terms to zero.

5 Finite element discretisation

The discretisation of the equilibrium equations is performed by employing the partition of unity property of finite element shape functions. In standard finite element methods, a smooth and continuous field $f(\mathbf{x},t)$ can be represented by discrete values a_i which are assigned to the nodes $i = 1..n_{nod}$ and corresponding finite element shape functions $\phi_i(\mathbf{x})$. It was shown by Babuška and Melenk [15] that when a field is not continuous, it can still be discretised using these standard finite element shape functions in combination with an enhanced basis function, according to:

$$f(\mathbf{x},t) = \sum_{i=1}^{n_{nod}} \phi_i(\mathbf{x}) \left(a_i(t) + \sum_{j=1}^{m} \gamma_j(\mathbf{x}) b_{ij}(t) \right), \qquad (10)$$

where $\gamma_j(\mathbf{x},t)$ is an enhanced basis with m orthogonal terms and b_{ij} are the additional nodal degrees of freedom that support the enhanced basis functions. The number m of enhanced base functions may be different for each node i in the model. However, in order to avoid linear dependency, the enhanced basis γ_j and the shape functions ϕ_i may not originate from the same span of functions. In this case, the enhanced basis functions $\gamma_j(\mathbf{x},t)$ are equal to the step functions $\mathcal{H}_{\Gamma_{\mathrm{d},j}}$. The total displacement field inside a specific continuum element can be written as:

$$\mathbf{u} = \mathbf{N}\mathbf{a} + \sum_{j=1}^{m} \mathcal{H}_{\Gamma_{\mathrm{d},j}} \mathbf{N}\mathbf{b}_j. \qquad (11)$$

where $\mathbf{N}$ is a matrix containing the shape functions ϕ_i for a the nodes that support this element [16]. The strain field as defined in equation (2) is equal to:

$$\boldsymbol{\varepsilon} = \mathbf{B}\mathbf{a} + \sum_{j=1}^{m} \mathcal{H}_{\Gamma_{\mathrm{d},j}} \mathbf{B}\mathbf{b}_j, \qquad (12)$$

where $\mathbf{B}$ contains the spatial derivatives of the shape functions. Finally, the magnitude of the jump in the displacement field $\mathbf{v}_j$ is equal to:

$$\mathbf{v}_j = \mathbf{N}\mathbf{b}_j. \qquad (13)$$

The admissible displacement fields as presented in equation (8) and their spatial derivatives can be discretised in a similar fashion. Substitution of these fields into (9) gives the discrete equilibrium equations. Details on this operation can be found in [2].

6 Implementation

The evolution of micro-cracks can be divided into three stages: the nucleation, the growth and finally the coalescence with other segments. In all cases, the same criterion is used to determine when and in which direction a segment is created or extended [2]. In order to arrive at a consistent numerical model, this fracture criterion is narrowly connected to the cohesive constitutive relation that governs the debonding process of a cohesive segment.

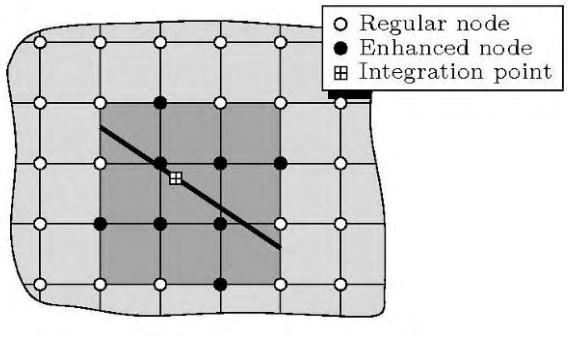

Figure 3: Creation of a new cohesive segment (bold line) in virgin material. The segment crosses the integration point in the bulk material in which the criterion was violated. The segment is stretched until it touches the boundary of the patch of elements (grey area) that share the nodes of the element in which the yield criterion was violated

When the stress state in a specific integration point in the bulk material exceeds the strength of the material, a new cohesive segment is added. The segment, which is assumed to be straight, crosses this integration point and is extended into the neighbouring elements until it touches the outer boundaries of these elements, see Figure 3. The patch of neighbouring elements consists of all elements that share one of the nodes of the central element that contains the integration point in which the criterion was violated. The nodes that support these outer boundaries are not enhanced in order to guarantee a zero crack opening at the tips of the new segments. When the stress state in the tip violates the fracture criterion for a specific angle, the segment is extended into the next element in that direction, until it touches the boundary of that element, see Figure 3.

A key feature of the method is the possibility of having multiple, interacting cohesive segments. To accommodate this, each cohesive segment is supported by a unique set of additional degrees of freedom. When two segments meet within a single element, the nodes that support the elements are enhanced twice. Consider the situation depicted in Figure 4, in which segment II is approaching another segment (I), which can either be a material interface or a previously created cohesive crack. When the fracture criterion at the tip of segment II is violated, the segment is extended accordingly. The position of segment I marks a discontinuity and can therefore be considered as a free edge in the material. Hence, segment two is only extended until it touches segment I, see Figure 4.

Since this segments forms a free edge, there is no new tip for segment II and all nodes of the corresponding element are enhanced.

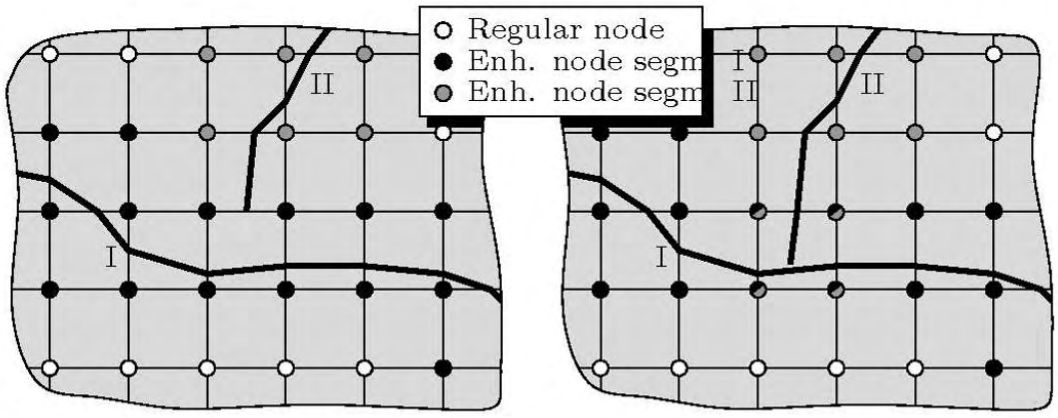

Figure 4: Merging of two cohesive segments (bold lines). Segment II is extended until it touches segment I (right picture). Segment I can be regarded as a free edge so that segment II will not have a tip in this case. Consequently, all nodes of the element will be enhanced in order to support displacement discontinuity of segment II. Note that the nodes of these elements are enhanced twice

To avoid sudden jumps in stresses when a discontinuity is inserted, the constitutive behaviour of the cohesive segment is related to the stress state in the bulk material that violates the fracture criterion. The initial normal and shear tractions, $t_{n,0}$ and $t_{s,0}$, respectively, are taken to be equal to corresponding the normal and shear tractions in the bulk material at the exact moment of nucleation [2,17].

When the normal traction component $t_{n,0}$ is positive, the cohesive segment is assumed to open as a mode-I crack. The cohesive tractions in both normal and shear directions t_n and t_s decrease monotonically from their initial values $t_{n,0}$ and $t_{s,0}$ to zero as a function of the normal displacement jump:

$$t_n = t_{n,0}\left(1-\frac{v_n}{v_{n,cr}}\right); \qquad t_s = t_{s,0}\left(1-\frac{v_n}{v_{n,cr}}\right) sgn(v_s), \qquad (14)$$

where v_n and v_s are the normal and sliding component of the displacement jump $\mathbf{v}$ respectively, see equation (3) and $sgn(\,)$ is the signum function:

$$sgn(x) = \frac{x}{|x|}. \quad (1)$$

The characteristic length of the cohesive law is determined by the critical normal opening displacement $v_{\mathrm{n},cr}$ at which the crack has fully developed and the tractions have reduced to zero. This parameter is related to the fracture toughness $\mathcal{G}_c$, or the area under the softening curve and can be determined as follows:

$$v_{\mathrm{n},cr} = \frac{2\mathcal{G}_c}{t_{\mathrm{n},0}}. \qquad (15)$$

When after some opening displacement $v_{\mathrm{n},1}$, the crack starts to close due to local unloading, the following relation is applied:

$$t_{\mathrm{n}} = t_{\mathrm{n},0}\left(1-\frac{v_{\mathrm{n},1}}{v_{\mathrm{n},cr}}\right)\frac{v_{\mathrm{n}}}{v_{\mathrm{n},1}}; \qquad t_{\mathrm{s}} = t_{\mathrm{s},0}\left(1-\frac{v_{\mathrm{n},1}}{v_{\mathrm{n},cr}}\right)\frac{v_{\mathrm{n}}}{v_{\mathrm{n},1}}sgn(v_{\mathrm{s}}). \qquad (16)$$

Once the normal displacement jump exceeds the critical opening $v_{\mathrm{n},cr}$, the crack has fully opened and the tractions in both normal and shear directions are set to zero.

7 Example

The performances of the cohesive segment are demonstrated in the following example, which is obtained from [18]. Here, the cohesive segments method is used in an explicit time integration scheme to simulate fast crack propagation. Details on the implementation can be found in [2].

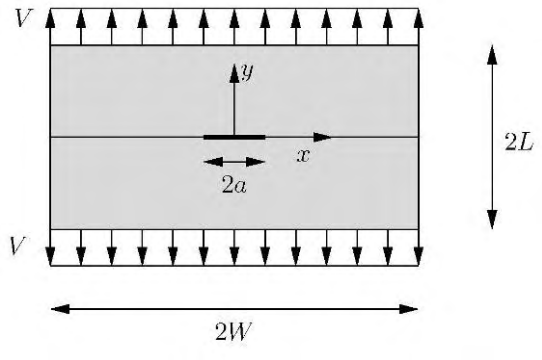

Figure 5: Geometry and loading conditions of the interface crack growth specimen

The specimen in Figure 5 consists of two parts with different elastic material properties that are bonded along $y = 0$ with a centre crack along the bond line. The dimensions of the specimen are $2W = 12$ mm and $2L = 6$ mm. The centre crack measures $2a = 2$ mm. The top and bottom edges of the specimen are subjected to impact loads that are modelled as

prescribed velocities that increase linearly to a value $V = 20$ m/s with a rise time $t_r = 10^{-7}$ s.

The top part of the specimen is made of a material with Young's modulus $E = 3.24 \cdot 10^9$ N/m^2. The Poisson's ratio is $\nu = 0.3$ and the density is $\rho = 1190$ kg/m^3. The material properties of the lower part are: $E = 12.2 \cdot 10^9$ N/m^2, $\nu = 0.3$ and $\rho = 1190$ kg/m^3, respectively. The interface is represented by a cohesive segment which is placed in the mesh beforehand. Debonding of this interface is governed by a mixed-mode cohesive constitutive relation [12] with $t_{max} = 3.24 \cdot 10^8$ N/m^2 and $\mathcal{G}_c = 700$ N/m. At the initially debonded part, a traction free constitutive relation is used. In the simulation, cracks are allowed to nucleate in the top half of the specimen only. Here, the fracture properties are $t_{max} = 410 \cdot 10^6$ N/m^2 and $\mathcal{G}_c = 700$ N/m. Because of symmetry along the y-axis, only one half of the specimen is modelled. The relatively coarse mesh consists of 39×39 four node elements, the time step chosen to be $\Delta t = 1.0 \cdot 10^{-9}$ s.

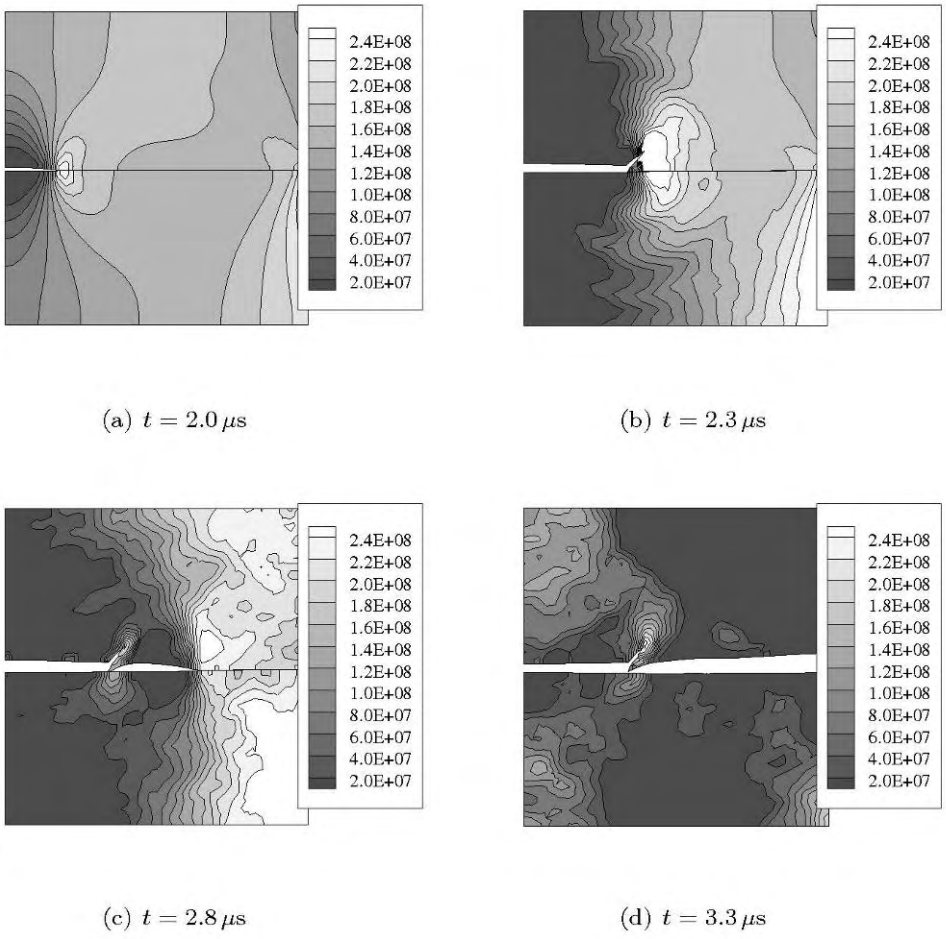

Figure 6: Evolution of fracture in the bi-material specimen The colour gradient represents the σ_{yy} stresses N/m^2. (a) Onset of debonding at the interface. (b) Creation of a new cohesive segment in the bulk material. This new segment is created at an angle of 68° with respect to the interface. (c) Continuation of debonding of the interface as a daughter crack ahead of the current crack tip. (d) Total failure of the specimen [18].

Upon loading, after approximately $t = 2.0\mu$s, the interface starts to debond, see Figure 6(a). The stress state around the crack tip soon builds up to a level such that a new cohesive segment nucleates in the top half of the specimen, Figure 6(b). This segment crosses the interface at an angle of approximately 68° with the interface. According to the implementation as described in the previous chapter, this new segment has a finite length of two elements. During the creation and opening of this branch, the debonding of the interface arrests. The new cohesive segment opens completely but is not extended and the branch seems to arrest. Instead, after some time, the interface starts to debond away from the branch position as a so-called daughter crack, similar to the fracture patterns in [19], Figure 6(c). After 3.3μs the interface has completely debonded and the specimen has lost its load carrying capability.

8 Conclusions

The ability to simulate crack growth in arbitrary directions is an important prerequisite to arrive at an objective numerical tool for the analysis of self-healing mechanisms in composite materials. The cohesive segments method is able to predict multiple interacting crack trajectories, irrespective of the structure of the finite element mesh. The next step is to extend this method with a numerical model for fluid flow in both porous constituents of the material (which plays an eminent role in autonomous healing processes in concrete) and through the cracks. The recently developed two-scale approach for fluid flow in fracture porous media, which is based on the partition of unity method as well, seems to be an ideal candidate for this [6]. Finally, when the healing agent has been transported to the fractured areas, the cohesive constitutive relations can be reversed to simulate rebonding of the crack surfaces. This final step will be the most challenging one in the development of the numerical tool, since it requires the understanding of the effects of chemical reaction on the mesoscopic level of observation. Initially, an empirical approach will be used [7].

REFERENCES

[1] White SR, Sottos NR, Geubelle PH, Moore JS, Kessler MR, Sriram SR, Brown EN and Viswanathan S (2001) Autonomic healing of polymer composites, Nature, 409: 794-797.

[2] Remmers JJC (2006) Discontinuities in Materials and Structures, A unifying computational approach. Ph.D. dissertation. Delft University of Technology, Delft, The Netherlands.

[3] Moës N, Dolbow J, Belytschko T (1999) A finite element method for crack growth without remeshing. International Journal for Numerical Methods in Engineering 46: 131--150.

[4] Wells GN and Sluys LJ (2001) A new method for modelling cohesive cracks using finite elements. International Journal for Numerical Methods in Engineering 50 (12): 2667--2682.

[5] Lewis RW, Schrefler BA. The Finite Element Method in the Static and Dynamic Deformation and Consolidation of Porous Media. John Wiley & Sons, Chichester, Second Edition, 1998.

[6] Réthoré J, de Borst R and Abellan MA (2007) A two-scale approach for fluid flow in fractured porous media. submitted to *International Journal for Numerical Methods in Engineering*.

[7] Schimmel EC and Remmers JJC (2006) Development of a constitutive model for self-healing materials. Report DACS-06-003, ISSN 1574-6992.

[8] Dugdale DS (1960) Yielding of steel sheets containing slits. Journal of the Mechanics and Physics of Solids 8: 100-108.

[9] Barenblatt GI (1962) The mathematical theory of equilibrium cracks in brittle fracture. Advances in Applied Mechanics 7: 55-129.

[10] Needleman A (1987) A continuum model for void nucleation by inclusion debonding. Journal of Applied Mechanics 54: 525--531

[11] Xu XP and Needleman A (1993) Void nucleation by inclusion debonding in a crystal matrix. Modelling and Simulation in Materials Science and Engineering 1: 111-132.
[12] Xu XP, Needleman A (1994) Numerical simulations of fast crack growth in brittle solids. Journal of the Mechanics and Physics of Solids 42: 1397-1434
[13] Tijssens MGA, Sluys LJ and van der Giessen E (2001) Simulation of fracture in cementitious composites with explicit modeling of microstructural features. Engineering Fracture Mechanics 68: "1245-1263.
[14] Schellekens JCJ and de Borst R (1992) On the numerical integration of interface elements. International Journal for Numerical Methods in Engineering 36 (1): 43--66.
[15] Babu s̆ ka I and Melenk J M (1997) The partition of unity method. International Journal for Numerical Methods in Engineering 40 (4): 727--758.
[16] Bathe KJ (1996) Finite Element Procedures. Prentice Hall, Upper Saddle River, NJ, USA.
[17] Camacho GT and Ortiz M (1996) Computational modelling of impact damage in brittle materials. International Journal of Solids and Structures 33: 2899--2938.
[18] Remmers JJC, de Borst R and Needleman A (2007) The simulation of dynamic crack propagation using the cohesive segments method. submitted to Journal of the Mechanics and Physics of Solids.
[19] Coker D, Rosakis AJ and Needleman A (2003) Dynamic crack growth along a polymer composite-homalite interface. Journal of the Mechanics and Physics of Solids 51 (3): 425-460.